Photoreceptors generate neuronal diversity in their target field through a Hedgehog morphogen gradient in *Drosophila*

Matthew P. Bostock and Vilaiwan M. Fernandes*.

Department of Cell and Developmental Biology, University College London, Gower Street, London, WC1E 6DE.

*Corresponding author; vilaiwan.fernandes@ucl.ac.uk

Abstract:

Defining the origin of neuronal diversity is a major challenge in developmental neurobiology. The *Drosophila* visual system is an excellent paradigm to study how cellular diversity is generated during development. Photoreceptors from the eye disc grow their axons into the optic lobe and secrete Hedgehog (Hh) to induce the lamina, such that for every unit eye there is a corresponding lamina unit made up of post-mitotic precursors stacked into columns. Each differentiated column contains five lamina neuron types (L1-L5), making it the simplest neuropil in the optic lobe, yet how this diversity is generated was unknown. Here, we found that Hh pathway activity is graded along the distal-proximal axis of lamina columns and further determined that this gradient in pathway activity arises from a gradient of Hh ligand. We manipulated Hh pathway activity both cell-autonomously in lamina precursors and by inactivating the Hh ligand, and showed that different thresholds of activity specify unique cell identities, with more proximal cell types specified in response to progressively lower Hh levels. Thus, our data establish that Hh acts as a morphogen to pattern the lamina. Although, this is the first such report during *Drosophila* nervous system development, our work uncovers a remarkable similarity with the vertebrate neural tube, which is patterned by Sonic Hedgehog. Altogether, we show that differentiating neurons can regulate the neuronal diversity of their distant target fields through morphogen gradients.

Introduction:

Our nervous systems are composed of more unique cell types than any other organ. This diversity is believed to underlie our ability to process sensory input and perform complex specialized tasks. Invertebrates and vertebrates deploy common developmental strategies to diversify neural cell types (Holguera and Desplan, 2018). To explore these, we used the complex but tractable visual system of *Drosophila melanogaster,* which is organized into repeated modular circuits that map the visual field.

The *Drosophila* visual system is composed of the compound eyes and optic lobes, which together contain ~200 neuronal cell types (Fischbach and Dittrich, 1989; Özel et al., 2020). Each optic lobe is made up of four distinct neuropils, the lamina, medulla, lobula and lobula plate. With ~100 cell types, the medulla is the most diverse and complex (Fischbach and Dittrich, 1989; Özel et al., 2020). Despite this, work in recent years has uncovered that the interplay between spatial patterning, temporal patterning and Notch-mediated binary fate decisions accounts for medulla diversity (Bertet et al., 2014; Erclik et al., 2017; Gold and Brand, 2014; Konstantinides et al., 2021; Li et al., 2013). In contrast, much less is known about how diversity is generated in the arguably simpler lamina, which contains only 5 neuronal cell types (L1-L5).

The lamina is the first neuropil to receive input from the photoreceptors and its development is linked to and dependent on photoreceptor development (Huang et al., 1998; Huang and Kunes, 1998, 1996; Sugie et al., 2010; Umetsu et al., 2006; Yogev et al., 2010). Photoreceptors are born progressively in the wake of a wave of differentiation that sweeps across the eye disc (Fig. 1A) (Roignant and Treisman, 2009). Two photoreceptor-derived signals, Hedgehog (Hh) and the Epidermal Growth Factor (EGF) Spitz, drive lamina development (Huang et al., 1998; Huang and Kunes, 1998, 1996; Sugie et al., 2010; Umetsu et al., 2006; Yogev et al., 2010). First, Hh signalling induces neuroepithelial cells to adopt lamina precursor cell (LPC) identity and express the lamina marker Dachshund (Dac), promotes their terminal divisions and regulates their adhesion and assembly into columns (*i.e.* ensembles of stacked LPC cell bodies associated with photoreceptor axon bundles; Fig. 1A, B) (Huang and Kunes, 1998, 1996; Sugie et al., 2010; Umetsu et al., 2006). Second, photoreceptor-derived EGF is required for LPCs to initiate neuronal differentiation (indicated by expression of the pan-neuronal marker Embryonic lethal abnormal vision [Elav]; Fig. 1A, B) (Huang et al., 1998; Yogev et al., 2010); however, this communication is indirect and involves a signalling relay through multiple glial populations, which ultimately induce lamina neuron differentiation through Mitogen Activated Protein Kinase (MAPK) signalling (Fig. 1A) (Fernandes et al., 2017; Prasad et al., 2021). Lamina neuron identities are invariant and stereotyped according to their position along the distal-proximal axis of columns; LPCs in the distal-most positions of columns will differentiate into L2s, followed by L3s, then L1s, then L4s, and finally L5s are positioned at the proximal end of columns (Fig. 1A, C) (Pecot et al., 2014). In addition, a combination of markers allow us to distinguish lamina neuron types: Sloppy paired 2 (Slp-2) alone labels L2s and L3s, Brain specific homeobox (Bsh) alone labels L4s, Seven up (Svp) together with Slp-2 labels L1s, and Slp-2 together with Bsh label L5s (Fig. 1A,C) (Pecot et al., 2014). The LPCs positioned between L4s

and L5s do not differentiate but instead are fated to die by apoptosis (Fig. 1A). Given that MAPK signalling drives differentiation in the lamina indiscriminately for all neuronal types (Fernandes et al., 2017; Prasad et al., 2021), how these neurons acquire their individual identities has remained elusive.

Here we showed that Hh signalling activity is graded from high to low along the distal-proximal axis of lamina columns. We examined the distribution of Hh ligand in the lamina and detected a protein gradient decreasing from a high point at the distal end of columns, consistent with the observed gradient of pathway activity. We then used genetic manipulations to modulate Hh signalling activity cell autonomously in LPCs or to disrupt Hh ligand directly and showed that different activity thresholds specify LPCs with distinct identities such that progressively decreasing Hh activity results in more and more proximal neuron identities being specified. These data establish that Hh is a morphogen in the lamina. Since photoreceptors are the sole source of Hh to the optic lobes at these developmental stages (Huang and Kunes, 1996), our data imply that in addition to inducing LPCs, promoting their assembly into columns and triggering their differentiation through glial signalling relays (Fernandes et al., 2017; Huang et al., 1998; Huang and Kunes, 1998, 1996; Prasad et al., 2021; Umetsu et al., 2006), photoreceptors also determine the neuronal diversity of the lamina. This is the first example of a morphogen patterning neuronal fates in *Drosophila*; it highlights a remarkable similarity with the ventral neural tube of vertebrates where a gradient of the morphogen Sonic Hedgehog, a Hh homologue, diversifies cell types (Placzek and Briscoe, 2018).

Results and Discussion:

Hh pathway activity is graded along the distal-proximal axis of LPC columns

For clues into how lamina neuron types are diversified, we integrated published single-cell RNA sequencing datasets at developmental timepoints that span lamina development (Konstantinides et al., 2021; Kurmangaliyev et al., 2020; Özel et al., 2020) (Fig. S1A; See Materials and Methods). As published previously, on uniform manifold approximation and projection (UMAP) visualizations L1, L2, L3 and L4 neuronal clusters were closer to each other than they were to the L5 cluster (Özel et al., 2020). The LPC cluster was connected to differentiated neurons by two streams of cells - one leading to the L1-L4 clusters and the other leading to the L5 cluster (Fig. 1D). Such convergent streams in UMAP visualizations are thought to represent intermediate states between progenitors and differentiated cells, suggesting that L1-L4 and L5 neurons have distinct developmental trajectories arising from a common pool of LPCs (Konstantinides et al., 2021; Özel et al., 2020). To test this, we used mitotic recombination to label the lineages of neuroepithelial cells with low induction frequency. These clones labelled compact patches of lamina cells, indicating that there is relatively little cell mixing (Fig. S1B-C; 13/13 clones). Importantly, the lineages of individual neuroepithelial cells contained all the lamina neuron types, including L5s, thus indicating that all lamina neurons have the same developmental origin (Fig. S2B,C; 13/13 clones; See Supplementary text).

We asked which transcripts distinguished L5 precursors from L1-L4 precursors, and, surprisingly, we found that several well-established Hh signalling targets were expressed at higher levels in the L1-L4 stream compared with the L5 stream, suggesting that L5 precursors experience lower Hh signalling than other lamina precursors. These included the direct transcriptional target *patched (ptc),* as well as *single-minded (sim), rhomboid (rho)* and *Zinc finger homeodomain 1 (zfh1)* (Fig. 1E-H) (Albert et al., 2018; Biehs et al., 2010; Chen and Struhl, 1996; Umetsu et al., 2006). Indeed, a transcriptional reporter for *ptc (ptc-lacZ)* was expressed at lower levels in L5 neurons compared with L1-L4 neurons (Fig. 1I,J; N=10). Consistent with the transcriptomic data, *ptc-lacZ* expression eventually decreased in older neurons (Figs. 1E,I,J; N=10). Importantly, in young columns prior to neuronal differentiation, we observed a gradient of *ptc-lacZ* expression, which was highest in the distal lamina and decreased along the distal-proximal axis (quantified in Fig. 1J with summary statistics from a mixed effects linear model in Table S1). Sim expression showed a similar distribution (Fig. S1D; N=14). These data indicate that Hh pathway activity is graded in the lamina, with the highest levels in the distal lamina and the lowest levels in the proximal lamina.

Hh::GFP is distributed in a protein gradient in the lamina

We sought to determine if graded Hh pathway activity in the lamina arises from a concentration gradient of Hh ligand. We analysed the distribution of a Hh::GFP fusion protein expressed under the control of endogenous enhancers of the *hh* locus and inserted into the genome using a Bacterial Artificial Chromosome in single copy (Chen et al., 2017). This transgene was previously reported to rescue a *hh* amorph, indicating that it is a functional *hh* allele (Chen et al., 2017). Interestingly, although Hh::GFP was present in photoreceptor cell bodies in the eye disc and in photoreceptor axons in the optic stalk, we detected much fainter expression in the axons once they reached the lamina (Fig. 2A; N=18). We measured GFP mean fluorescence intensity (MFI) as a function of distal-proximal distance for the two youngest lamina columns (See Materials and Methods) and, strikingly, observed a gradient of MFI polarised from high to low with increasing distance from the distal to proximal ends of columns (Fig. 2B-C; N=10). These measurements do not distinguish between intracellular and extracellular Hh::GFP, but instead represent total Hh::GFP. Nonetheless, these data indicate that Hh ligand is present in a distal-to-proximal gradient in the lamina, consistent with the gradient in Hh pathway activity along lamina columns and suggest that ligand availability is responsible for the activity gradient.

High and low extremes of Hh pathway activity cell-autonomously specify distal and proximal lamina neuron identities, respectively.

Hh signalling is known to trigger the early steps of lamina development, including promoting early lamina marker expression such as *dac* and *sim*, as well as promoting terminal LPC divisions and column assembly (Huang and Kunes, 1998, 1996; Sugie et al., 2010; Umetsu et al., 2006). However, no role for Hh in lamina neuron specification or differentiation has been

identified thus far. In the vertebrate neural tube, a gradient of Sonic Hedgehog (Shh) signalling specifies ventral progenitor identities (Placzek and Briscoe, 2018), therefore, we wondered whether the graded Hh pathway activity we observed could specify neuronal identity in LPCs; in particular, we hypothesised that low Hh signalling levels in LPCs specify proximal neuron identity (*i.e.* L5s) and high Hh signalling levels specify distal neuron identity (*i.e.* L2s). To test this, we sought to disrupt Hh signalling cell autonomously in the lamina and assess the effects on lamina neuron specification. When we blocked Hh pathway activity completely in clones mutant for *smoothened (smo),* we did not recover any Dac-expressing LPCs (Fig. S2A; N=15), consistent with previous reports (Huang and Kunes, 1998, 1996). Therefore, to reduce Hh pathway activity partially we used a lamina-specific driver (*R27G05-Gal4*), which drives expression in Dac-expressing LPCs exiting the posterior lamina furrow (Fig. S2B), to express a repressor form of the transcriptional effector of Hh signalling, Cubitus interruptus (Ci; referred to as Ci^{rep}) (Busson and Pret, 2007). We restricted Gal4 activity temporally using a temperature sensitive Gal80 (see Materials and Methods). Expressing Ci^{rep} in LPCs led to a 2.9-fold increase in the proportion of Bsh and Slp-2 double-positive L5s relative to controls, while the proportion of other lamina neuron subtypes was reduced relative to controls (Figs. 3A,B,D-H and S2C-F; Kruskal-Wallis H test; $P<0.0001$; N=10). Moreover, whereas in control laminas L5s were only observed as a single row in the proximal lamina, expressing Ci^{rep} caused Bsh and Slp-2 double-positive L5s to be distributed along the entire distal-proximal lengths of columns (Fig. 3B, N=10). Similarly, knocking down Ci in the lamina by RNA interference (Ci^{RNAi}) (Fig. 3C; N=9) resulted in ectopic L5s (2.2-fold increase relative to controls, Kruskal-Wallis H test; $P<0.0001$) and a reduction in the number of L2/L3s and L4 lamina neurons (Figs. 3D-H and S2C-F, Kruskal-Wallis H test; $P^{L2/L3}<0.0001$, $P^{L1}<0.05$ and $P^{L4}<0.0001$). Thus, decreasing Hh signalling autonomously within LPCs was sufficient to induce the proximal cell identity (L5s), throughout the distal-proximal lengths of columns and at the expense of other neuronal types.

We next asked whether increasing Hh signalling autonomously would specify LPCs to differentiate with distal lamina neuron identity (*i.e.* L2). We generated LPCs with a gain-of-function in Hh pathway activity by inducing positively-labelled clones (Lee and Luo, 2001) that were homozygous mutant for the negative Hh pathway regulator *ptc* (Chen and Struhl, 1996; Kalderon, 2005). *ptc* mutant clones never contained L5s (Slp-2 and Bsh co-expressing cells), L4s (Bsh-only expressing cells) or L1s (Svp and Slp-2 co-expressing cells), but instead only contained neurons singly positive for Slp-2, indicative of L2/L3 identity (Fig. 3I-J; 17/17 clones from 15 optic lobes). Thus, increasing Hh signalling in the lamina results in L2/L3 specification at the expense of L1, L4 and L5 specification. In summary, disrupting Hh signalling activity cell autonomously to either low or high extremes specified LPCs with either the most proximal or distal lamina neuron identities, respectively.

Titrating functional Hh availability favours distinct neuronal types at different thresholds

The data presented thus far are consistent with Hh acting as a morphogen to specify cell identities in the lamina, *i.e.* in a concentration-dependent manner, however, our cell-autonomous

manipulations only determined the impact of experiencing either the high or low extremes of pathway activity on lamina neuron identity specification. To demonstrate that different thresholds of Hh ligand determine lamina neuron identities, we sought to manipulate Hh directly and to differing degrees of severity. We predicted that, if Hh was acting as a morphogen, progressively reducing Hh levels should result in progressively more proximal fates. To do so, we used animals harbouring a temperature sensitive loss of function allele of *hh* (hh^{ts2}), which we raised at the permissive temperature (18˚C) and then shifted to the restrictive temperature (29˚C) for either 6 hours, 12 hours, 24 hours, 45 hours or 72 hours before dissecting at the white prepupal stage (Figs. 4A-G, S3A-J). Consistent with the known role of Hh signalling in photoreceptor and early lamina development (Huang and Kunes, 1996), we recovered fewer and fewer photoreceptors and lamina neurons with increasing lengths of temperature shifts (Fig. S3A-J), with no LPCs or L-neurons recovered for the 45- and 72-hour temperature shifts (Fig. 4F,G) (Huang and Kunes, 1996). These results indicated that our perturbations effectively titrated the availability of functional Hh with longer periods at the restrictive temperature. Next, we used lamina neuron type-specific markers to evaluate neuronal cell types under these conditions. We found that the proportion of L2/L3s (Slp-2 single positive neurons) decreased as the availability of functional Hh was titrated to lower and lower levels, whereas the proportion of L5s (Slp-2 and Bsh double-positive neurons) increased (Figs. 4A-E; quantified in Fig. 4I-L; Kruskal-Wallis H test; $P<0.0001$). Importantly, the proportion of L1s (Slp-2 and Svp double positive neurons) increased for the 6-hour temperature shift before decreasing with longer temperature shifts. Thus, L1 neurons, which normally occupy intermediate lamina column positions were favoured at the expense of distal neuron types at intermediate thresholds of Hh pathway activity (Fig. 4C, J; Kruskal-Wallis H test; $P<0.0001$). Notably, under these conditions L1 and L5s were no longer confined to their normal positions within lamina columns but were observed throughout (Fig. 4A-D). Altogether our data establish that Hh acts as a morphogen to diversify lamina neuron types.

Here we uncovered a previously unknown role for Hh as a morphogen that specifies lamina neuron identities, thus revealing yet another layer of dependence of lamina development on photoreceptors-derived signals. It will be important to test whether differential Hh signalling levels alone specify all five neuronal identities or whether additional inputs are needed together with Hh signalling. This is the first report of a morphogen patterning neuronal fates in *Drosophila*. It highlights the remarkable evolutionary conservation of this developmental strategy, which is widespread in vertebrates (Placzek and Briscoe, 2018; Sagner and Briscoe, 2019).

Nonetheless, it is not obvious how the Hh gradient is established in the lamina, such that it is polarised from high to low along the distal-proximal lengths of lamina columns, as photoreceptor axons themselves span this full distance. Axonal trafficking of Hh was shown to be regulated by an evolutionarily conserved motif in its cleaved C-terminal domain (Chu et al., 2006; Daniele et al., 2017), disruption of which affected neuronal diversity in the lamina

specifically (Chu et al., 2006). This indicates that axonal trafficking may play a role in establishing the Hh gradient, however, more work is required to uncover the exact molecular mechanisms involved. It is unexpected that neurons, here photoreceptors, define the neuronal diversity of their target field, and raises the possibility that neurons in other contexts could also be patterning their target fields during development through morphogen gradients. Indeed, many vertebrate neuronal types express Shh (Dakubo et al., 2003; Farmer et al., 2016; Garcia et al., 2010; Gonzalez-Reyes et al., 2012; Harwell et al., 2012; Petralia et al., 2011; Wallace, 1999), however, their ability to generate instructive gradients to pattern distant neural fields has not been determined thus far.

References

Albert EA, Puretskaia OA, Terekhanova N V, Labudina A. 2018. Direct control of somatic stem cell proliferation factors by the Drosophila testis stem cell niche **145**:dev156315. doi:10.1242/dev.156315

Bertet C, Li X, Erclik T, Cavey M, Wells B, Desplan C. 2014. Temporal Patterning of Neuroblasts Controls Notch-Mediated Cell Survival through Regulation of Hid or Reaper. *Cell* **158**:1173–1186. doi:10.1016/j.cell.2014.07.045

Biehs B, Kechris K, Liu S, Kornberg TB. 2010. Hedgehog targets in the Drosophila embryo and the mechanisms that generate tissue-specific outputs of Hedgehog signaling. *Development* **137**:3887–3898. doi:10.1242/dev.055871

Busson D, Pret A. 2007. GAL4/UAS Targeted Gene Expression for Studying Drosophila Hedgehog Signaling. *Methods Mol Biol* **397**:161–201.

Chen W, Huang H, Hatori R, Kornberg TB. 2017. Essential basal cytonemes take up Hedgehog in the Drosophila wing imaginal disc. *Development* **144**:3134–3144.

Chen Y, Struhl G. 1996. Dual Roles for Patched in Sequestering and Transducing Hedgehog **87**:553–563.

Chu T, Chiu M, Zhang E, Kunes S. 2006. A C-Terminal Motif Targets Hedgehog to Axons , Coordinating Assembly of the Drosophila Eye and Brain. *Dev Cell* **10**:635–646.

Dakubo GD, Wang YP, Mazerolle C, Campsall K, Mcmahon AP, Wallace VA. 2003. Retinal ganglion cell-derived sonic hedgehog signaling is required for optic disc and stalk neuroepithelial cell development. *Development* **130**:2967–2980.

Daniele JR, Chu T, Kunes S. 2017. A novel proteolytic event controls Hedgehog intracellular sorting and distribution to receptive fields. *Biol Open* **6**:540–550.

Erclik T, Li X, Courgeon M, Bertet C, Chen Z, Baumert R, Ng J, Koo C, Arain U, Behnia R, Del A, Rodriguez V, Senderowicz L, Negre N, Kevin P. 2017. Integration of temporal and spatial patterning generates neural diversity. *Nat Publ Gr* **541**:365–370. doi:10.1038/nature20794

Farmer WT, Abrahamsson T, Chierzi S, Lui C, Zaelzer C, Jones E, Ponroy Bally B, Chen GG, Theroux J-F, Pend J, Bourque CW, Charron F, Ernst C, Sjöström J, Murai KK. 2016. Neurons diversify astrocytes in the adult brain through sonic hedgehog signaling. *Science (80-)* **351**:849–854.

Fernandes VM, Chen Z, Rossi AM, Zipfel J, Desplan C. 2017. Glia relay differentiation cues to coordinate neuronal development in Drosophila. *Science (80-)* **357**:886–891.

Fischbach KF, Dittrich APM. 1989. The optic lobe of Drosophila melanogaster. I: A. Golgi analysis of wild-type structure. *Cell Tissue Res* **258**:441–475. doi:doi: 10.1007/BF00218858

Garcia ADR, Petrova R, Eng L, Joyner AL. 2010. Sonic Hedgehog Regulates Discrete Populations of Astrocytes in the Adult Mouse Forebrain **30**:13597–13608. doi:10.1523/JNEUROSCI.0830-10.2010

Gold KS, Brand AH. 2014. Optix defines a neuroepithelial compartment in the optic lobe of the Drosophila brain Optix defines a neuroepithelial compartment in the optic lobe of the Drosophila brain. *Neural Dev* **9**:18.

Gonzalez-Reyes LE, Verbitsky M, Blesa J, Jackson-lewis V, Paredes D, Tillack K, Phani S, Kramer ER, Przedborski S, Kottmann AH. 2012. Sonic Hedgehog Maintains Cellular in the Adult Nigrostriatal Circuit. *Neuron* **75**:306–319.

Harwell CC, Parker PRL, Gee SM, Okada A, Mcconnell SK, Kreitzer AC. 2012. Sonic Hedgehog Expression in Corticofugal Projection Neurons Directs Cortical Microcircuit Formation. *Neuron* **73**:1116–1126. doi:10.1016/j.neuron.2012.02.009

Holguera I, Desplan C. 2018. Neuronal specification in space and time. *Science (80-)* **362**:176–180.

Huang Z, Kunes S. 1998. Signals transmitted along retinal axons in Drosophila: Hedgehog signal reception and the cell circuitry of lamina cartridge assembly. *Development* **125**:3753–64. doi:10.1016/s0092-8674(00)80094-x

Huang Z, Kunes S. 1996. Hedgehog, transmitted along retinal axons, triggers neurogenesis in the developing visual centers of the Drosophila brain. *Cell* **86**:411–22. doi:10.1016/S0092-8674(00)80114-2

Huang Z, Shilo BZ, Kunes S. 1998. A retinal axon fascicle uses spitz, an EGF receptor ligand, to construct a synaptic cartridge in the brain of Drosophila. *Cell* **95**:693–703. doi:10.1016/S0092-8674(00)81639-6

Kalderon D. 2005. The mechanism of hedgehog signal transduction. *Biochem Soc Trans* **33**:1509–1512. doi:10.1042/BST0331509

Konstantinides N, Rossi AM, Escobar A, Dudragne L, Chen Y-C, Tran T, Martinez A, Özel MN, Simon F, Shao Z, Nadejda M, Fullard JF, Walldorf U, Roussos P, Konstantinides N, Jaimes AM, Özel MN, Simon F, Shao Z, Tsankova NM, Fullard JF, Walldorf U, Roussos P, Desplan C. 2021. A comprehensive series of temporal transcription factors in the fly visual system. *bioRxiv*:2021.06.13.448242. doi: 10.1101/2021.06.13.448242

Kurmangaliyev YZ, Yoo J, Valdes-aleman J, Sanfilippo P, Zipursky SL, Kurmangaliyev YZ, Yoo J, Valdes-aleman J, Sanfilippo P, Zipursky SL. 2020. Transcriptional Programs of Circuit Assembly in the Drosophila Visual System. *Neuron* **108**:1045–1057. doi:10.1016/j.neuron.2020.10.006

Lee T, Luo L. 2001. Mosaic analysis with a repressible cell marker (MARCM) for Drosophila neural development. *Trends Neurosci* **24**:251–4.

Li X, Chen Z, Desplan C. 2013. Temporal patterning of neural progenitors in drosophila, 1st ed, Current Topics in Developmental Biology. Elsevier Inc. doi:10.1016/B978-0-12-396968-2.00003-8

Özel MN, Simon F, Jafari S, Holguera I, Chen Y, Benhra N, El-danaf RN, Kapuralin K, Malin JA, Konstantinides N, Desplan C. 2020. Neuronal diversity and convergence in a visual system developmental atlas. *Nature* **589**:88–95. doi:10.1038/s41586-020-2879-3

Pecot M, Chen Y, Akin O, Chen Z, Tsui CYK, Zipursky SL. 2014. Sequential axon-derived signals couple target survival and layer specificity in the drosophila visual system. *Neuron* **82**:320–333. doi:10.1016/j.neuron.2014.02.045

Petralia RS, Wang Y, Mattson MP, Yao PJ, Petralia RS, Wang Y, Mattson MP, Yao PJ. 2011.

Sonic hedgehog distribution within mature hippocampal neurons. *Comun Integr Biol* **4**:775–777. doi:10.4161/cib.17832

Placzek M, Briscoe J. 2018. Sonic hedgehog in vertebrate neural tube development. *Int J Dev Biol* **62**:225–234.

Prasad AR, Lago-Baldaia I, Bostock MP, Housseini Z, Fernandes VM. 2021. Differentiation signals from glia are fine-tuned to set neuronal numbers during development. *bioRxiv* 2021.12.13. doi: 10.1101/2021.12.13.472383

Roignant J-Y, Treisman JE. 2009. Pattern formation in the Drosophila eye disc. *Int J Dev Biol* **53**:795–804. doi:10.1387/ijdb.072483jr

Sagner A, Briscoe J. 2019. Establishing neuronal diversity in the spinal cord : a time and a place. *Development* **146**:dev182154. doi:10.1242/dev.182154

Sugie A, Umetsu D, Yasugi T, Fischbach K-F, Tabata T. 2010. Recognition of pre- and postsynaptic neurons via nephrin/NEPH1 homologs is a basis for the formation of the Drosophila retinotopic map. *Development* **137**:3303–3313. doi:10.1242/dev.047332

Umetsu D, Murakami S, Sato M, Tabata T. 2006. The highly ordered assembly of retinal axons and their synaptic partners is regulated by Hedgehog/Single-minded in the Drosophila visual system. *Development* **133**:791–800. doi:10.1242/dev.02253

Wallace VA. 1999. Purkinje-cell-derived Sonic hedgehog regulates granule neuron precursor cell proliferation in the developing mouse cerebellum. *Curr Biol* **9**:445–448.

Yogev S, Schejter ED, Shilo BZ. 2010. Polarized secretion of drosophila EGFR ligand from photoreceptor neurons is controlled by ER localization of the ligand-processing machinery. *PLoS Biol* **8**:e1000505.

Acknowledgements:

We thank C. Desplan, D. Kalderon, B. Shilo, G. Struhl and J. Treisman for reagents, and S. Ackerman, M. Amoyel, B. Conradt, C. Desplan, A. Franz, P. Salinas, A. Rossi, C. Stern, L. Venkatasubramanian and members of the Fernandes labs for comments on the manuscript. Stocks obtained from the Bloomington Drosophila Stock Center (NIH P40OD018537) were used in this study. Monoclonal antibodies obtained from the Developmental Studies Hybridoma Bank, created by the NICHD of the NIH and maintained at The University of Iowa, were used in this study.

Competing interests:

Authors declare that they have no competing interests.

Funding:

Wellcome Trust Sir Henry Dale Research Fellowship 210472/Z/18/Z (VMF), UCL Biosciences Graduate Research Scholarship (MPB).

Author contributions:

Conceptualization: VMF, MPB

Investigation: MPB

Supervision: VMF
Writing – original draft: VMF
Writing – review & editing: MPB, VMF

Supplementary Materials
Supplementary text
Materials and Methods
Table S1to S2
Supplementary References
Figs. S1 to S3

1 **Fig 1.**

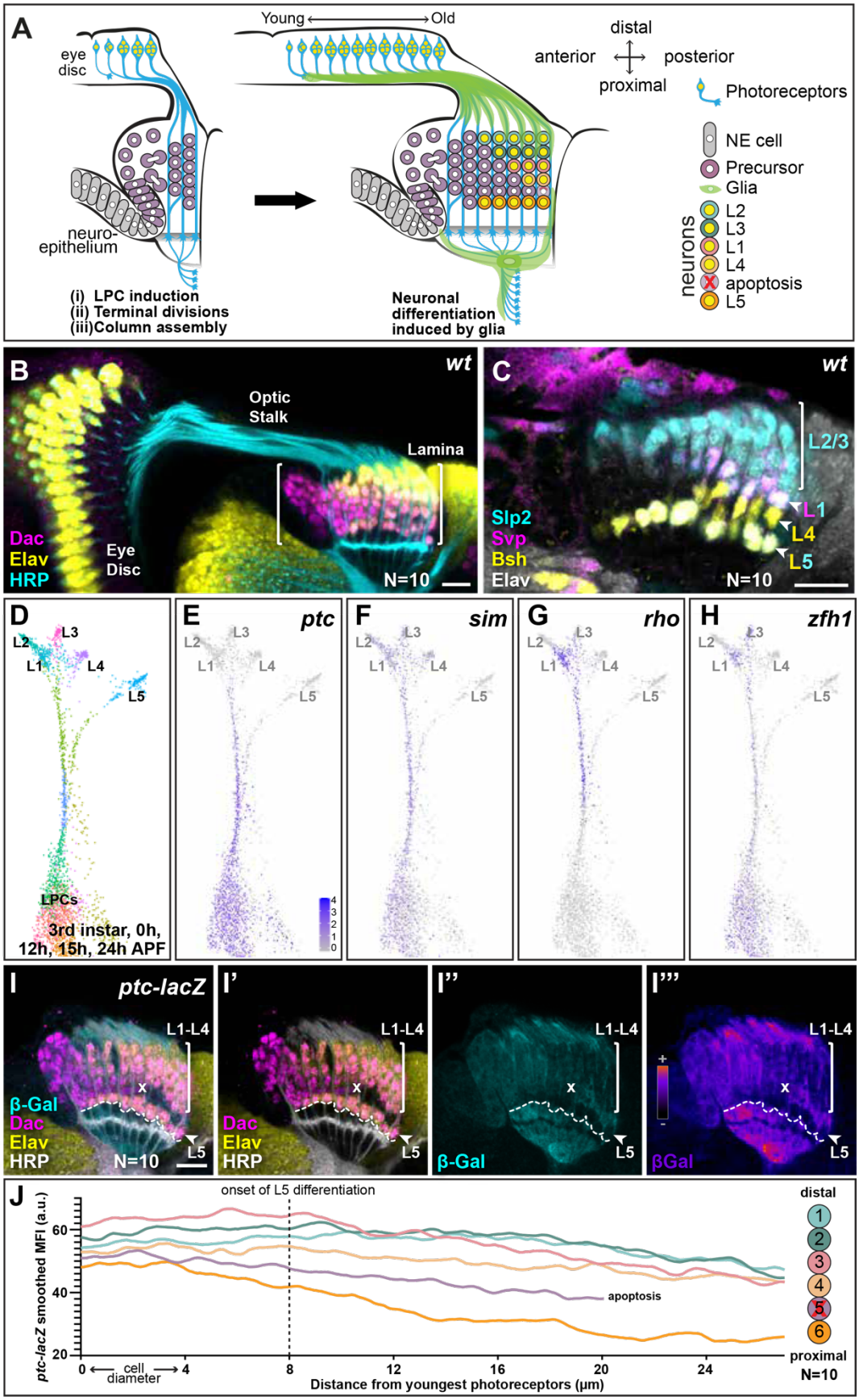
A
Young
Old
eye disc
neuro-epithelium
(i) LPC induction
(ii) Terminal divisions
(iii)Column assembly
Neuronal differentiation induced by glia
distal
anterior
posterior
proximal
Photoreceptors
NE cell
Precursor
Glia
neurons
L2
L3
L1
L4
apoptosis
L5
B
wt
Optic Stalk
Lamina
Dac
Elav
HRP
Eye Disc
N=10
C
wt
L2/3
Slp2
Svp
Bsh
Elav
L1
L4
L5
N=10
D
L2
L3
L1
L4
L5
LPCs
3rd instar, 0h, 12h, 15h, 24h APF
E
ptc
F
sim
G
rho
H
zfh1
I
ptc-lacZ
L1-L4
β-Gal
Dac
Elav
HRP
N=10
I'
I''
I'''
βGal
J
onset of L5 differentiation
ptc-lacZ smoothed MFI (a.u.)
cell diameter
Distance from youngest photoreceptors (μm)
apoptosis
distal
proximal
N=10

Fig. 1: Hh pathway activity is graded along lamina columns. (A) Schematic of the developing lamina. Photoreceptor axons release Hh into the optic lobe which guides lamina development by driving neuroepithelial cells to develop into lamina precursor cells (LPCs), their terminal divisions and column assembly. Once assembled into columns of six LPCs each, LPCs differentiate into five distinct neuron types (L1-L5) in response to MAPK activity that is induced by signals from glia(Fernandes et al., 2017; Prasad et al., 2021). Lamina neuron types are positioned stereotypically along the distal to proximal axis of columns: L2, L3, L1, L4, L5; the LPCs between L4s and L5s undergo apoptosis. **(B)** A wildtype optic lobe and eye disc, with the developing lamina labelled by Dac (magenta), differentiating neurons by Elav (yellow) and photoreceptor axons by Horse Radish Peroxidase (HRP, cyan). **(C)** A wildtype lamina labelled with lamina neuron-type-specific markers, Slp-2 (cyan), Bsh (yellow), and Svp (magenta); all neurons are marked by Elav (white). Slp-2 alone labels L2s and L3s, Bsh alone labels L4s, Svp together with Slp-2 label L1s, and Slp-2 together with Bsh label L5s. **(D)** UMAP visualisation of LPCs, differentiated L1-L5 neurons and intermediate stages of differentiation using 150 principal components calculated on the log-normalized integrated gene expression from single-cell RNA sequencing datasets of the third larval instar, 0 hours-, 12 hours-, 15 hours- and 24 hours-APF. See Figure S1A for full integrated dataset. **(E-H)** UMAP visualisation from (D; grey) showing log normalised expression of the Hh signalling targets (blue): **(E)** *ptc*, **(F)**, *sim*, **(G)** *rho* and **(H)** *zfh1,* which all show higher levels of expression in the convergent stream connecting the LPC cluster with mature L1-L4 neuron clusters rather than the stream connecting the LPC cluster with the L5 neuron cluster. **(I)** An optic lobe expressing *ptc-LacZ* stained for β-Galactosidase (β-Gal; cyan), Dac (magenta), Elav (yellow) and HRP (white). **(I”’)** shows (I”) in pseudo-colour. Dashed line marks the most proximal surface of the lamina. “x” marks the point from which the excess LPCs have been cleared. In young columns, β-Gal expression decreases along the distal to proximal axis, being lowest in the proximal lamina. L5s have the lowest levels of β-Gal, which eventually decreases in older L1-L4s. **(J)** Smoothed (second order with 6 neighbours; See Materials and methods) mean fluorescence intensities (MFIs; arbitrary units; a.u.) of *ptc-LacZ* (β-Gal) by distal to proximal cell position as indicated. L5s and the excess LPCs began with and maintained the lowest levels of β-Gal expression over time. Summary statistics for the raw data in Table S1. Scale bar = 20µm.

1 **Fig. 2**

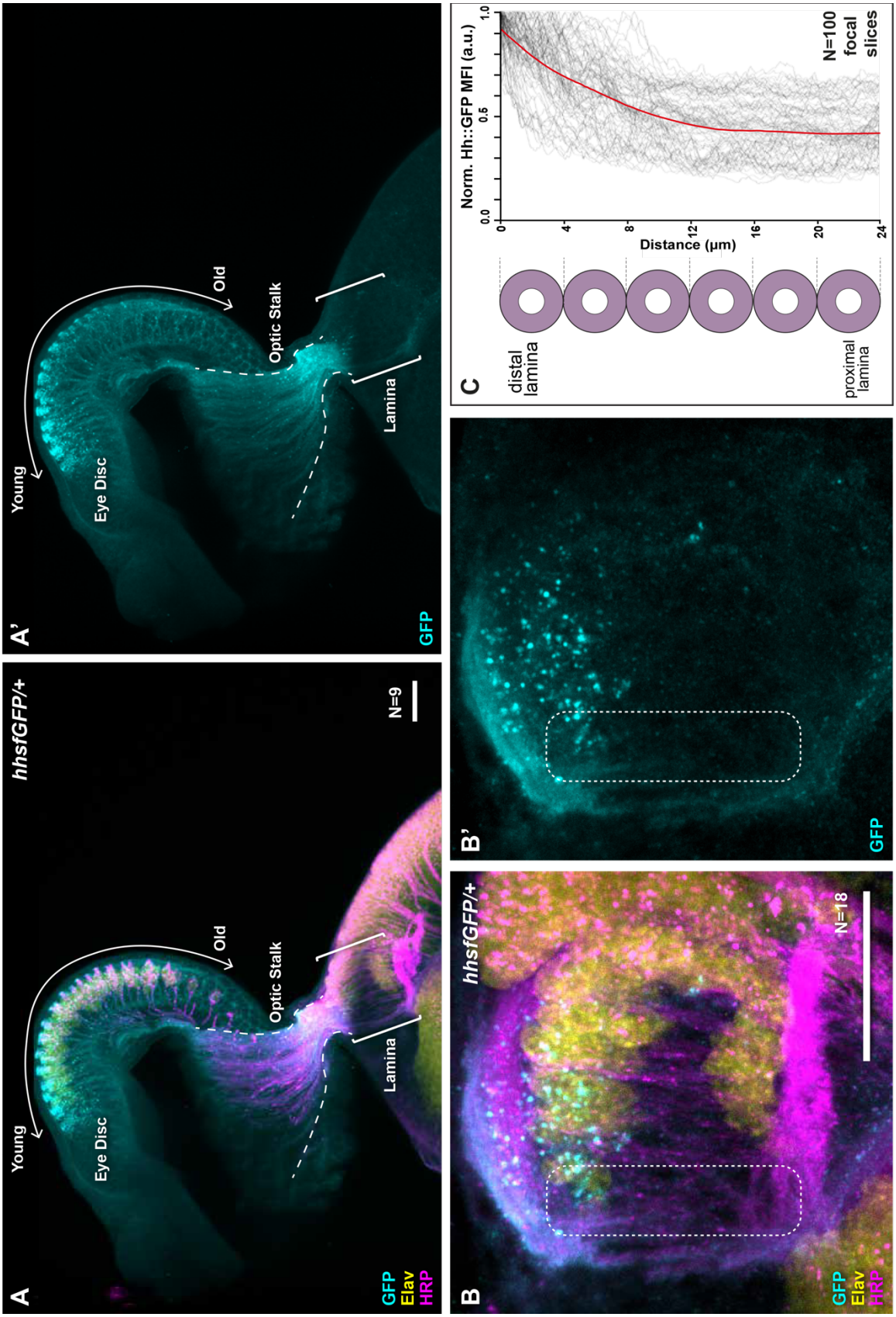
A
hhsfGFP/+
Young
Old
Eye Disc
Optic Stalk
Lamina
N=9
GFP
Elav
HRP
A'
GFP
B
hhsfGFP/+
N=18
GFP
Elav
HRP
B'
GFP
C
distal lamina
proximal lamina
Norm. Hh::GFP MFI (a.u.)
0.0
0.5
1.0
Distance (µm)
0
4
8
12
16
20
24
N=100 focal slices

Fig. 2: Hh::GFP is distributed in a protein gradient in the lamina. (A) A maximum intensity projection of an *hh-sfGFP* optic lobe and eye disc complex, where *hh-sfGFP* encodes Hh tagged with superfolder GFP. Hh::GFP (cyan) was present in photoreceptor cell bodies in the eye disc (Elav, yellow), with higher levels in younger photoreceptors as reported previously(Huang and Kunes, 1996) and photoreceptor axons in the optic stalk (HRP; magenta). Hh::GFP expression decreases rapidly once photoreceptors enter the lamina (brackets). **(B)** A maximum intensity projection of a *hh-sfGFP* lamina oriented to view the lamina in cross-section. Hh::GFP puncta were visible more prominently in the distal lamina, with fewer and smaller puncta appearing in proximal regions. **(C)** Mean fluorescence intensity (MFI) plots normalised to the maximum MFI value for each plot (arbitrary units; a.u.) of Hh::GFP as a function of distance from distal to proximal cell position as indicated from the two youngest lamina columns (dashed outline in B). The red line shows regression averaging of each of the MFI profiles (see Materials and Methods). Scale bar = 20µm.

1 **Fig. 3**

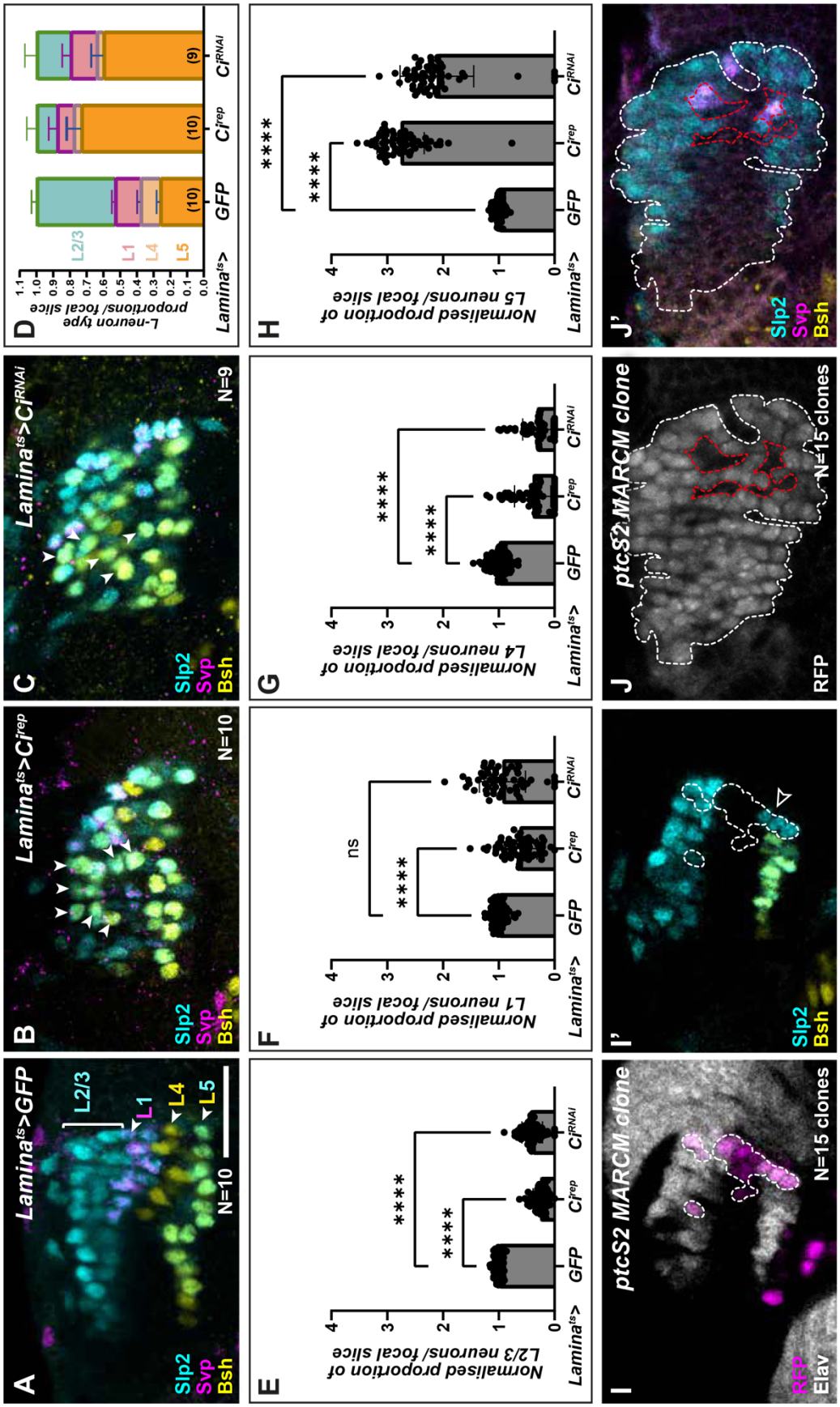
A
Lamina^ts>GFP
L2/3
L1
L4
L5
Slp2
Svp
Bsh
N=10
B
Lamina^ts>Ci^rep
Slp2
Svp
Bsh
N=10
C
Lamina^ts>Ci^RNAi
Slp2
Svp
Bsh
N=9
D
L-neuron type proportions/ focal slice
L2/3
L1
L4
L5
(10)
(10)
(9)
Lamina^ts>
GFP
Ci^rep
Ci^RNAi
E
Normalised proportion of L2/3 neurons/ focal slice
****
****
F
Normalised proportion of L1 neurons/ focal slice
ns
****
G
Normalised proportion of L4 neurons/ focal slice
****
****
H
Normalised proportion of L5 neurons/ focal slice
****
****
I
ptcS2 MARCM clone
RFP
Elav
N=15 clones
I'
Slp2
Bsh
J
ptcS2 MARCM clone
RFP
N=15 clones
J'
Slp2
Svp
Bsh

Fig. 3: High and low extremes of Hh pathway activity specify distal and proximal lamina neuron identities, respectively. (A-C) Lamina-specific misexpression of **(A)** CD8::GFP (control), **(B)** Ci^{rep} and **(C)** Ci^{RNAi}, labelled with lamina neuron-type-specific markers Slp-2 (cyan), Bsh (yellow), and Svp (magenta). **(A)** The pattern of Slp-2, Bsh, and Svp expression was the same as the wildtype (Fig. 1C). Upon lamina-specific misexpression of (B) Ci^{rep} or (C) Ci^{RNAi}, ectopic Slp-2 and Bsh co-expressing cells (L5s) were recovered in the distal lamina (arrowheads). **(D)** Quantifications of the proportion of each lamina neuron type per focal slice aggregated for (A-C). (**E-F)** The same as (D), normalised to the control and split by lamina neuron type: (E) L2/L3s, (F) L1s, (G) L4s, (H) L5s (see Methods and Materials). Error bars represent Standard Deviation. Ns indicated in parentheses in (D). **(I)** An optic lobe with a small, RFP-positive ptc^{S2} MARCM clone labelled with **(I)** Elav (white) and RFP (magenta), **(I')** Slp-2 (cyan) and Bsh (yellow). Clones in the lamina are outlined by dashed lines. A clone that spanned the proximal lamina was still Elav and Slp-2 positive but lacked Bsh, indicating that cells were specified as L2/L3s and not L5s. **(J)** An optic lobe with a large, RFP-positive ptc^{S2} MARCM clone stained for **(J)** RFP (white), **(J')** Slp-2 (cyan), Bsh (yellow), and Svp (magenta). Clones in the lamina are outlined by dashed white lines. Cells contained within the lamina that are not part of the clone are outlined by dashed red lines. A clone that spanned the whole lamina was Slp-2 and Elav-positive, but not Svp or Bsh-positive indicating that the cells had differentiated into L2s or L3s but not L1s, L4s or L5s. Note that the Svp-positive cells are not contained within the clone. Scale bar = 20µm.

1 **Fig. 4**

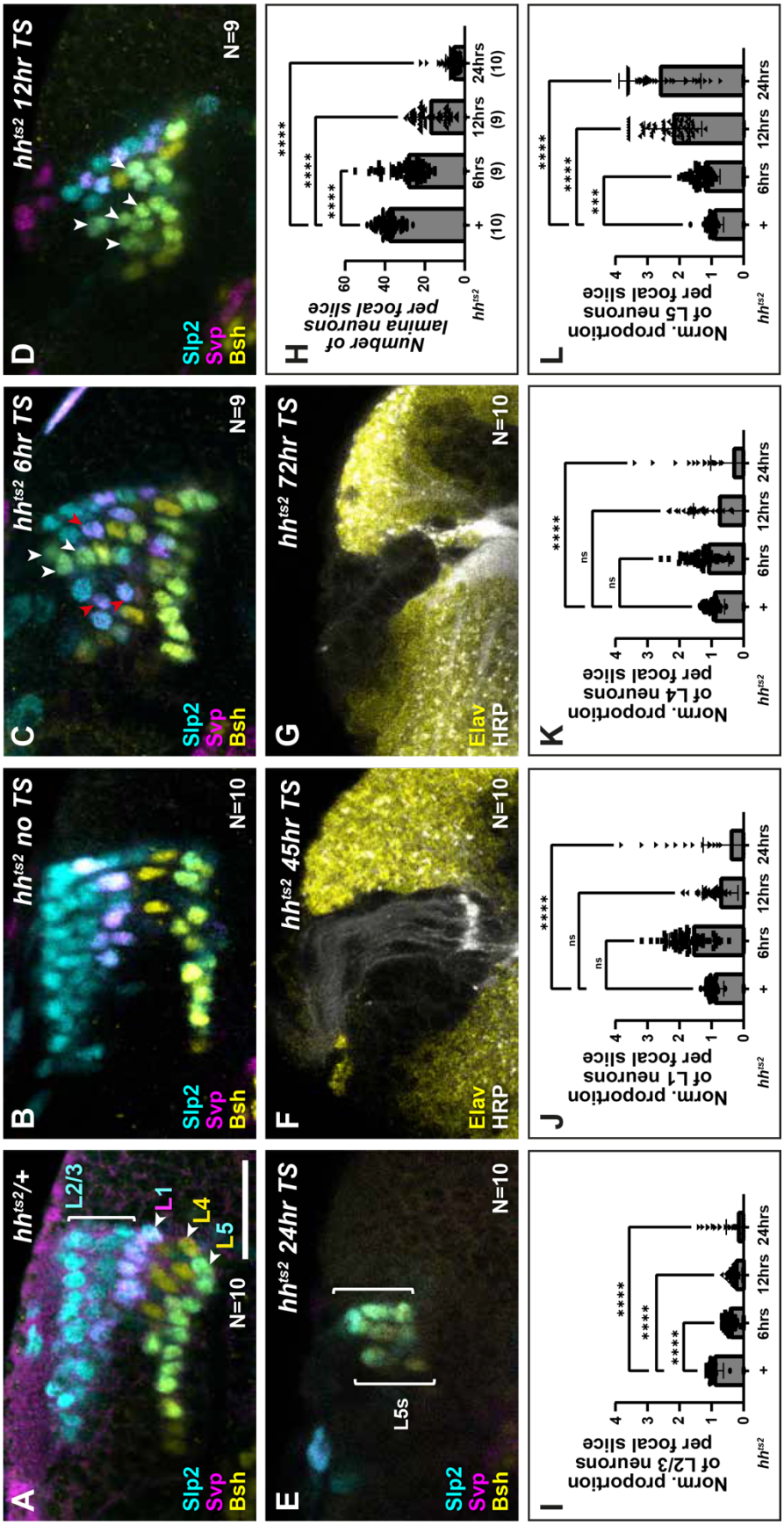
A
hhts2/+
L2/3
L1
L4
L5
N=10
Slp2
Svp
Bsh
B
hhts2 no TS
N=10
C
hhts2 6hr TS
N=9
D
hhts2 12hr TS
N=9
E
hhts2 24hr TS
L5s
N=10
F
hhts2 45hr TS
Elav
HRP
N=10
G
hhts2 72hr TS
N=10
H
Number of lamina neurons per focal slice
I
Norm. proportion of L2/3 neurons per focal slice
J
Norm. proportion of L1 neurons per focal slice
K
Norm. proportion of L4 neurons per focal slice
L
Norm. proportion of L5 neurons per focal slice
hhts2
+
6hrs
12hrs
24hrs
(10)
(9)
(10)
****
***
ns

Fig. 4: Titrating functional Hh availability favours distinct neuronal types at different thresholds. Laminas labelled with neuron-type-specific markers Slp-2 (cyan), Svp (magenta) and Bsh (yellow) in **(A)** hh^{ts2}/+ shifted from the permissive temperature (18ºC) to the restrictive temperature (29ºC) for 24 hours, **(B)** hh^{ts2} raised at the permissive temperature, **(C-G)** hh^{ts2} shifted from the permissive temperature to the restrictive temperature for **(C)** 6 hours, **(D)** 12 hours, **(E)** 24 hours. The pattern of neuronal differentiation worsened progressively with longer temperature shifts, with fewer neurons differentiating overall. Slp-2 and Bsh positive cells (L5s) were observed in the distal lamina (white arrowheads) for 6 hr, 12 hr and 24 hr temperature shifts, till most cells present differentiated into L5 neurons for the 24 hour temperature shift. Whereas Slp-2 and Svp co-expressing cells (L1) increased only for the 6 hr temperature shift and were distributed throughout the distal-proximal axis (red arrowheads). **(F,G)** hh^{ts2} shifted from the permissive temperature to the restrictive temperature for **(F)** 45 hours and **(G)** 72 hours stained for Elav (yellow) and HRP (white). A few photoreceptor bundles are present but no LPCs formed under the **(F)** 45 hour temperature shift condition, whereas neither photoreceptors nor LPCs were present for the **(G)** 72 hour temperature shift condition. **(H)** Quantification of the total number of lamina neurons (Elav-positive cells) per focal slice in hh^{ts2}/+ and hh^{ts2} shifted from the permissive temperature to the restrictive temperature as indicated. Error bars represent Standard Deviation. Ns indicated in parentheses. **(I-L)** Quantifications of the proportions of each lamina neuron subtype per slice and normalised to the control for each hh^{ts2} temperature shift condition. Scale bar = 20µm.

Supplementary Materials for

Photoreceptors generate neuronal diversity in their target field through a Hedgehog morphogen gradient in *Drosophila*

Matthew P. Bostock and Vilaiwan M. Fernandes*.

Department of Cell and Developmental Biology, University College London, Gower Street, London, WC1E 6DE.

*Corresponding author; vilaiwan.fernandes@ucl.ac.uk

Supplementary text

L1-L4 and L5 neurons do not have distinct developmental origins

Our analyses of the developmental single cell RNA sequencing (scRNAseq) data revealed that the cluster corresponding to lamina precursor cells (LPCs) was connected to the clusters corresponding to the lamina neurons by two separate streams of cells, one to L1-L4 clusters and one to the L5 cluster (Fig. 1D). Previously, Suzuki et al. (2016) proposed a model in which L5 neurons have a distinct developmental origin to the L1-L4 neurons, such that L5 neurons or the LPCs which differentiate into them, would arise from the dorsal and ventral tips of the lamina and migrate in, while the LPCs that differentiate into L1-L4 neurons would be born from the lamina furrow that spans the main lamina (Suzuki et al., 2016). To test this possibility, we induced single control MARCM clones per optic lobe in the neuroepithelium during the second larval instar and observed their neuronal make-up in the lamina at 0-5 hours after puparium formation (APF). If L5 neurons originate from the tips of the lamina, then we would expect clones induced in the central lamina to include L1-L4 but not L5 neurons. In contrast, clones remained largely intact, and we recovered L1-L5 neuron types as part of these clones (Fig. S1B, C; 13/13 clones). Thus, these data were inconsistent with the model in which L5s have a distinct developmental origin to the L1-L4 neurons.

Materials and Methods

Drosophila stocks and maintenance:

Drosophila melanogaster strains and crosses were reared on standard cornmeal medium and raised at 25˚C or 29˚C or shifted from 18˚C to 29˚C for genotypes as indicated in Table S2. We used the following mutant and transgenic flies in combination or recombined in this study (See Table S2 for more details; {} enclose individual genotypes, separated by commas):

Canton S, {*ptc-lacZ/TM6B*} (a gift from G. Struhl), {*ywhsflp*^{122}*, tub-gal4, UAS-GFP; FRT40A, Gal80/Cyo*} (a gift from F. Schweisguth), {*ey-Gal80; sp/Cyo;*} (BDSC: 35822), {*;Gal80ts; TM2/TM6B*} (BDSC: 7108), {*w*^{1118}*;; R27G05-Gal4*} (BDSC: 48073), {*;;UAS-CD8::GFP*} (gifts from C. Desplan), {*y*^{1} *sc** *v*^{1} *sev*^{21}*; Ci-RNAi*} (BDSC: 64928), {*UAS-Ci*^{76}} (a gift from J. Treisman), {*y*^{1}*; FRT42D, ptc*^{S2}*/CyO*} (BDSC: 6332), {*ywhsflp*^{122}*, tub-gal4, UAS-RFP; FRT42D, Gal80/Cyo*} (a gift from G. Struhl), {*FRT40A, smo*^{3}*/ CyO*} (a gift from C. Boekel), {*w***; UAS-cos.N; MKRS/TM6B*} (BDSC: 55039), {*yw*^{1118}*; hh::sfGFP*} (BDSC: 86271), {*w*^{1118}*; hh*^{ts2} *e*^{s}*/TM6B*} (BDSC: 1684).

<u>*Mosaic analysis:*</u>

We generated *smo*^{3} and *ptc*^{S2} MARCM (Figs. S2A and 3I,J, respectively) clones by heat-shocking larvae 2 days after egg laying (AEL) at 37˚C for 90 minutes. To generate one wild-type MARCM clone per lamina (Fig. S1B,C), we heat-shocked larvae (1 day AEL) for 60 minutes at 37˚C. All MARCM crosses were raised at 25˚C until dissection at 0-5 hours after puparium formation (APF).

<u>*Immunocytochemistry, antibodies and microscopy:*</u>

We dissected eye-optic lobe complexes from early pupae (0-5hrs APF) in 1X phosphate-buffered saline (PBS), fixed in 4% formaldehyde for 20 minutes, blocked in 5% normal donkey serum and incubated in primary antibodies diluted in block for 2 nights at 4˚C. Samples were then washed in 1X PBS with 0.5% TritonX (PBSTx), incubated in secondary antibodies diluted in block, washed in PBSTx and mounted in SlowFade (Life Technologies).

We used the following primary antibodies in this study: mouse anti-Dac$^{2-3}$ (1:20, Developmental Studies Hybridoma Bank; DSHB), rat anti-Elav (1:100, DSHB), mouse anti-Elav (1:20, DSHB), mouse anti-Svp (1:50, DSHB), rabbit anti-Slp-2 (1:100; a gift from C. Desplan), rabbit-Bsh (1:500; a gift from C. Desplan), mouse anti β-galactosidase (1:500; Promega #Z3781), chicken anti-GFP (1:400; EMD Millipore), mouse anti-Sim (1:20; a gift from T. Tabata), chicken anti-RFP (1:500; Rockland #600-901-379s), rabbit-anti-GFP (1:500; Thermofisher #A6455), AlexaFluor405 conjugated Goat Anti-HRP (1:100; Jackson Immunolabs), AlexaFluor405-, Cy3-, or AlexaFluor647- conjugated Goat Anti-HRP (1:200; Jackson Immunolabs). Secondary antibodies were obtained from Jackson Immunolabs or Invitrogen and used at 1:800. Images were acquired using Zeiss 800 and 880 confocal microscopes with 40X objectives.

<u>*scRNAseq analyses:*</u>

To maximize temporal resolution during development as well as the number of cells analysed, we combined three publicly available scRNAseq datasets of optic lobes from the following developmental timepoints: wandering third instar larva, 0 hours after puparium formation (APF), 12 hours APF, 15 hours APF and 24 hours APF. We combined these datasets using the Seurat v.3 integration pipeline to remove batch effects between libraries(Stuart et al.,

2019) as follows: Using the default parameters in Seurat 4.0.1 we first normalised each dataset with the NormaliseData function. Next, we extracted the 2000 most variable features with the FindVariableFeatures function. We then integrated the data using the FindIntegrationAnchors and IntegrateData functions. Next, we clustered the integrated dataset using the following functions: ScaleData, RunPCA (using 150 principal components as in(Konstantinides et al., 2021)), FindNeighbours (80 dimensions), FindClusters (resolution = 5), RunUMAP.

We annotated clusters corresponding to lamina cell types based on a combination of previous annotations from the source datasets (Özel et al., 2020) and known markers: *dac, eya, tll, gcm* for lamina precursor cells; *svp* and *slp2* for L1s; *slp2* for L2s; *erm* and *slp2 for L3s*; *bsh and apterous for L4s*; *bsh* and *slp2 for L5s* (Chotard et al., 2005; Guillermin et al., 2015; Hasegawa et al., 2013; Huang and Kunes, 1996; Piñeiro et al., 2014; Tan et al., 2015).

To analyse differentially expressed genes between the L1-L4 and the L5 convergent stream, we first used the CellSelector function to manually select the two streams as two individual clusters. Next, we used the FindMarkers (two-sided Wilcox rank-sum test) function with default parameters to identify positively or negatively expressed genes based on log fold change. To visualise UMAPs and gene expression, we used the DimPlot and FeaturePlot functions.

Quantification and Statistical analyses:

We used Fiji-ImageJ(Schindelin et al., 2012) or Imaris (version x64-9.5.1) to process and quantify confocal images as described below. We used Adobe Photoshop and Adobe Illustrator software to prepare figures. We used GraphPad Prism8, JMP and R (version 4.0.3) software to perform statistical tests. In all graphs, whiskers indicate the standard deviation. N values are indicated on graphs.

Mean Fluorescence Intensity (MFI) quantifications and statistical analyses:

Ptc-lacZ: Using Fiji-ImageJ, we selected the 10 most centrally located focal slices of the lamina (*ptc-lacZ;* Fig. 1I; step size = 1μm) using photoreceptor axons (HRP), and the lobula plug (Dac expression) as landmarks. We then obtained average intensity projections of these and generated MFI profile plots by measuring *β*-Gal MFI from the youngest lamina column to the oldest column for each of the 6 rows (distal-proximal cell positions) of the lamina.
We used a mixed effects linear model in JMP to test for an interaction between *ptc-lacZ (β-Gal)* Mean Fluorescence Intensity, distal-to-proximal cell position and along the anterior-posterior axis starting from the first column (Summary Statistics are provided in Table S1). We used GraphPad Prism8 to apply a moving average of 6 neighbours to smooth the data, which are plotted in Fig. 1J.

Hh-sfGFP/+: As above, we obtained 10 centrally located focal slices and measured the MFI profiles along the distal-proximal positions of the two youngest lamina columns (Fig. 2B,C). Using Dac expression to mark lamina precursors, the distal most lamina precursor was

taken as the starting position, with the most proximal lamina precursor as the final. We normalised each MFI profile to the maximum MFI value for each profile. We then performed regression averaging using *ggplot* in R to generate a smoothed average plot of Hh-sfGFP fluorescence based on the individual profiles.

Cell-type quantifications:

For *Lamina*^{ts}*>CD8::GFP, Ci*^{rep}*, Ci*^{RNAi}, and *hh*^{ts2} experiments, lamina subtypes were identified using the markers Slp-2, Svp and Bsh. We were unable to distinguish between L2 and L3 neurons since both express Slp-2 only. We quantified the number of L2/L3s, L1s, L4s and L5s in 10 centrally located optical slices in 10 optic lobes. Since total lamina neuron numbers were also affected by Hh pathway manipulations, we calculated the proportion of each lamina neuron type relative to the total number of neurons and plotted these normalised to the control in Figs. 3 and 4. Fig. S2 shows the raw numbers of each lamina neuron type in each focal slice for each condition.

Table S1. Mixed effects linear model summary statistics for *ptc-lacZ (β-Gal)* MFI as a function of Distance and Cell position (distal-proximal).

Source	F Ratio	Prob > F
Distance (μm)	7744.904	<.0001
Cell position	2320.251	<.0001
(Distance)*(Cell position)	191.2012	<.0001

Table S2. List of genotypes and conditions used for all experiments

(Note that only female genotypes are listed though both sexes were included in our analyses)

Fig.	Panel	Genotype	Conditions
1	B	*Canton S*	Raised at 25ºC
1	C	*Canton S*	Raised at 25ºC
1	I	*;;ptc-lacZ*	Raised at 25ºC
2	A, B	*;hh-sfGFP/+;*	Raised at 25ºC
3	A	*ey-Gal80; Gal80ts; R27G05-Gal4/UAS-CD8::GFP*	Raised at 18ºC till late-L1, then shifted to 29ºC for 72 hours
3	B	*ey-Gal80; Gal80ts; R27G05-Gal4/UAS-Ci*^{rep}	Raised at 18ºC for 12 days and 21 hours, then shifted to 29ºC for 12 hours
3	C	*ey-Gal80; Gal80ts; R27G05-Gal4/UAS-Ci*^{RNAi}	Raised at 18ºC for 12 days, then shifted to 29ºC for 24 hours
3	I, J	*y,w,hsflp*^{122}*/+, Tub-Gal4, UAS-nls.GFP; FRT42D, Tub-Gal80 /FRT42D, ptc*^{S2}*;*	Raised at 25ºC before and after heat shocking. See

			Mosaic analysis for more detail.
4	A	*y,w;;hh^{ts2}/+ (24hrs ts)*	Raised at 18ºC for 13 days, then shifted to 29ºC for 24 hours
4	B	*y,w;;hh^{ts2}*	Raised at 18ºC for 14 days
4	C	*y,w;;hh^{ts2} (6h ts)*	Raised at 18ºC for 13 days, then shifted to 29ºC for 6 hours
4	D	*y,w;;hh^{ts2} (12h ts)*	Raised at 18ºC for 12 days and 21 hours, then shifted to 29ºC for 12 hours
4	E	*y,w;;hh^{ts2} (24h ts)*	Raised at 18ºC for 12 days, then shifted to 29ºC for 24 hours
4	F	*y,w;;hh^{ts2} (45h ts)*	Raised at 18ºC for 11 days, then shifted to 29ºC for 45 hours
4	G	*y,w;;hh^{ts2} (72h ts)*	Raised at 18ºC for 10 days, then shifted to 29ºC for 72 hours
S1	B, C	*w,hsflp^{122}/+, Tub-Gal4, UAS-nls.GFP; FRT40D, Tub-Gal80 /FRT40D;*	Raised at 25ºC before and after heat shocking. See Mosaic analysis in Materials and Methods for more detail.
S1	D	*Canton S*	Raised at 25ºC
S2	A	*y,w,hsflp^{122}/+, Tub-Gal4, UAS-nls.GFP; FRT42D, Tub-Gal80 /FRT40A, smo^{3};*	Raised at 25ºC before and after heat shocking. See Mosaic analysis for more detail.
S2	B	*ey-Gal80; Gal80ts; R27G05-Gal4/UAS-CD8::GFP*	Raised at 18ºC till late-L1, then shifted to 29ºC for 72 hours
S2	C	*ey-Gal80/+; tub-Gal80^{ts}/UAS-Cos2; R27G05/+*	Raised at 18ºC till late-L2, then shifted to 29ºC for 48 hours
S3	A-E, F- J	Same as 4A-G	Same as 4A-G

Supplementary References

Chotard C, Leung W, Salecker I. 2005. glial cells missing and gcm2 cell autonomously regulate both glial and neuronal development in the visual system of Drosophila. *Neuron* **48**:237–251. doi:10.1016/j.neuron.2005.09.019

Guillermin O, Perruchoud B, Sprecher SG, Egger B. 2015. Characterization of Tailless functions during drosophila optic lobe formation. *Dev Biol* **405**:202–213. doi:10.1016/j.ydbio.2015.06.011

Hasegawa E, Kaido M, Takayama R, Sato M. 2013. Brain-specific-homeobox is required for the specification of neuronal types in the Drosophila optic lobe. *Dev Biol* **377**:90–99. doi:10.1016/j.ydbio.2013.02.012

Huang Z, Kunes S. 1996. Hedgehog, transmitted along retinal axons, triggers neurogenesis in the developing visual centers of the Drosophila brain. *Cell* **86**:411–22. doi:10.1016/S0092-8674(00)80114-2

Konstantinides N, Rossi AM, Escobar A, Dudragne L, Chen Y-C, Tran T, Martinez A, Özel MN, Simon F, Shao Z, Nadejda M, Fullard JF, Walldorf U, Roussos P, Konstantinides N, Jaimes AM, Özel MN, Simon F, Shao Z, Tsankova NM, Fullard JF, Walldorf U, Roussos P, Desplan C. 2021. A comprehensive series of temporal transcription factors in the fly visual system. *bioRxiv*:2021.06.13.448242. doi: 10.1101/2021.06.13.448242

Kurmangaliyev YZ, Yoo J, Valdes-aleman J, Sanfilippo P, Zipursky SL, Kurmangaliyev YZ, Yoo J, Valdes-aleman J, Sanfilippo P, Zipursky SL. 2020. Transcriptional Programs of Circuit Assembly in the Drosophila Visual System. *Neuron* **108**:1045–1057. doi:10.1016/j.neuron.2020.10.006

Özel MN, Simon F, Jafari S, Holguera I, Chen Y, Benhra N, El-danaf RN, Kapuralin K, Malin JA, Konstantinides N, Desplan C. 2020. Neuronal diversity and convergence in a visual system developmental atlas. *Nature* **589**:88–95. doi:10.1038/s41586-020-2879-3

Piñeiro C, Lopes CS, Casares F. 2014. A conserved transcriptional network regulates lamina development in the Drosophila visual system. *Development* **141**:2838–47. doi:10.1242/dev.108670

Schindelin J, Arganda-carreras I, Frise E, Kaynig V, Longair M, Pietzsch T, Preibisch S, Rueden C, Saalfeld S, Schmid B, Tinevez J, White DJ, Hartenstein V, Eliceiri K, Tomancak P, Cardona A. 2012. Fiji : an open-source platform for biological-image analysis. *Nat Methods* **9**:676–682. doi:10.1038/nmeth.2019

Stuart T, Butler A, Hoffman P, Stoeckius M, Smibert P, Satija R, Stuart T, Butler A, Hoffman P, Hafemeister C, Papalexi E, Iii WMM, Hao Y, Stoeckius M, Smibert P, Satija R. 2019. Comprehensive Integration of Single-Cell Data Resource Comprehensive Integration of Single-Cell Data. *Cell* **177**:1888-1902.e21. doi:10.1016/j.cell.2019.05.031

Suzuki T, Hasegawa E, Nakai Y, Kaido M, Takayama R, Sato M. 2016. Formation of Neuronal Circuits by Interactions between Neuronal Populations Derived from Different Origins in the Drosophila Visual Center. *Cell Rep* **15**:499–509. doi:10.1016/j.celrep.2016.03.056

Tan L, Zhang KX, Pecot MY, Nagarkar-Jaiswal S, Lee PT, Takemura SY, McEwen JM, Nern A, Xu S, Tadros W, Chen Z, Zinn K, Bellen HJ, Morey M, Zipursky SL. 2015. Ig Superfamily Ligand and Receptor Pairs Expressed in Synaptic Partners in Drosophila. *Cell* **163**:1756–1769. doi:10.1016/j.cell.2015.11.021

1 **Fig. S1**

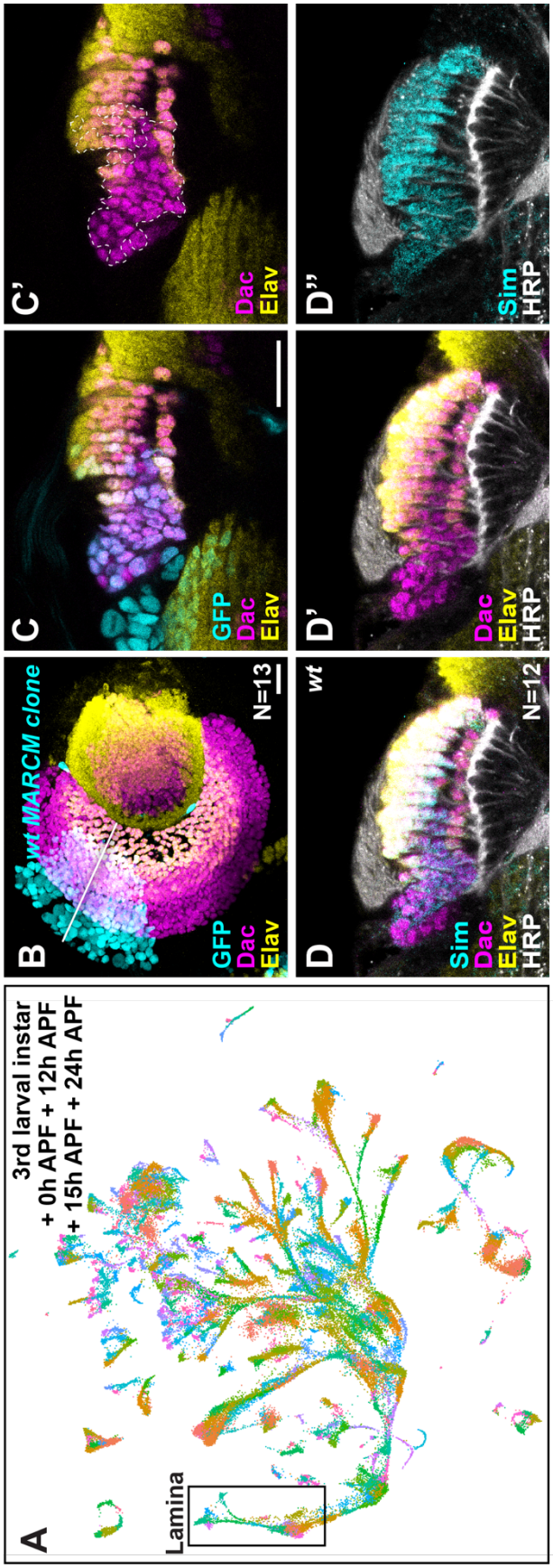
A
3rd larval instar
+ 0h APF + 12h APF
+ 15h APF + 24h APF
Lamina
B
wt MARCM clone
GFP
Dac
Elav
N=13
C
GFP
Dac
Elav
C'
Dac
Elav
D
wt
Sim
Dac
Elav
HRP
N=12
D'
Dac
Elav
HRP
D''
Sim
HRP

Fig. S1: L1-L4 and L5 neurons do not have distinct developmental origins

(A) UMAP visualisation of integrated third larval instar, 0 hours-, 12 hours-, 15 hours- and 24 hours-APF single cell RNA sequencing datasets(Konstantinides et al., 2021; Kurmangaliyev et al., 2020; Özel et al., 2020) using 150 principal components calculated on the log-normalized integrated gene expression. Rectangle marks LPCs and lamina neurons of varying maturity, which were identified based on known markers and existing annotations from the 15 hour APF dataset as described in Materials and Methods. **(B)** A lateral view of an optic lobe with a single wildtype MARCM GFP positive clone stained for GFP (cyan), Dac (magenta) and Elav (yellow). **(C)** A cross-sectional view through the clone shown in (B) shows LPCs and all L-neuron types included in the clone (dashed line in C'), indicating that all LPCs, which differentiate into L1-L5 are generated in the same way from the lamina furrow. **(D)** Wildtype optic lobes stained for Dac (magenta), HRP (white), Elav (yellow) and Sim (cyan). Sim expression was lowest in the proximal lamina. Scale bar = 20µm.

1 **Fig. S2**

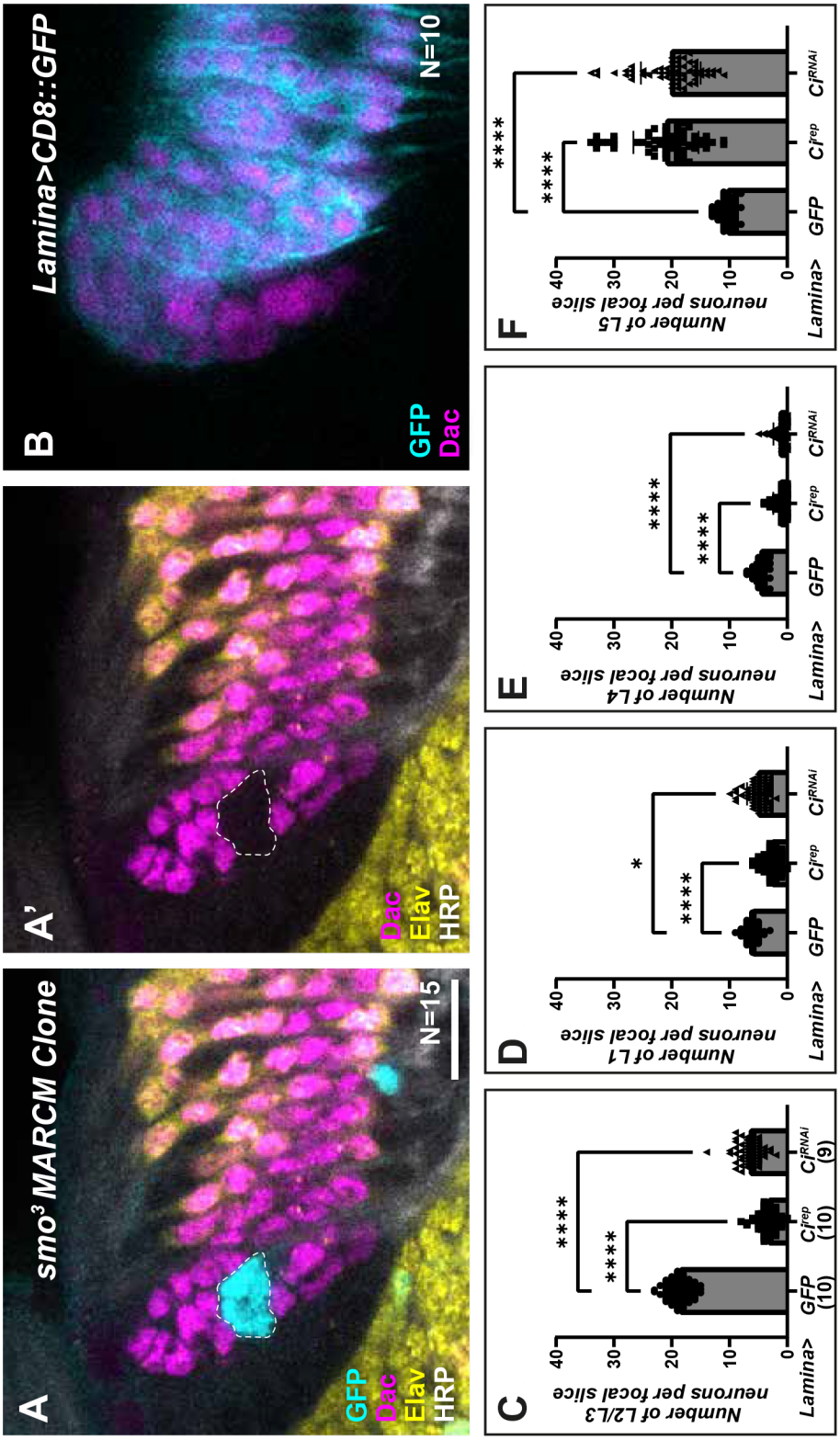
A
smo3 MARCM Clone
GFP
Dac
Elav
HRP
N=15
A'
Dac
Elav
HRP
B
Lamina>CD8::GFP
GFP
Dac
N=10
C
Number of L2/L3 neurons per focal slice
****
****
Lamina>
GFP (10)
Cj^rep (10)
Cj^RNAi (9)
D
Number of L1 neurons per focal slice
*
****
Lamina>
GFP
Cj^rep
Cj^RNAi
E
Number of L4 neurons per focal slice
****
****
Lamina>
GFP
Cj^rep
Cj^RNAi
F
Number of L5 neurons per focal slice
****
****
Lamina>
GFP
Cj^rep
Cj^RNAi

Fig. S2: Lamina-specific misexpression of *Ci*^{rep} and *Ci*^{RNAi} perturb specification. (A) An optic lobe with a GFP-positive (cyan) *smo*^{3} MARCM clone (dashed outline) labelled with Dac (magenta), Elav (yellow), and HRP (white). Cells within *smo*^{3} clones did not express Dac and did not incorporate into the lamina. **(B)** R27G05-Gal4, a lamina-specific Gal4 drove expression of CD8::GFP (cyan) and Dac (magenta). GFP expression was driven in LPCs exiting the lamina furrow. **(C-F)** Quantifications of the number of each lamina neuron type per focal slice, L2/L3, L1, L4, or L5, for each condition. Mean and Standard Deviation are indicated. Scale bar = 20μm.

1 **Fig. S3**

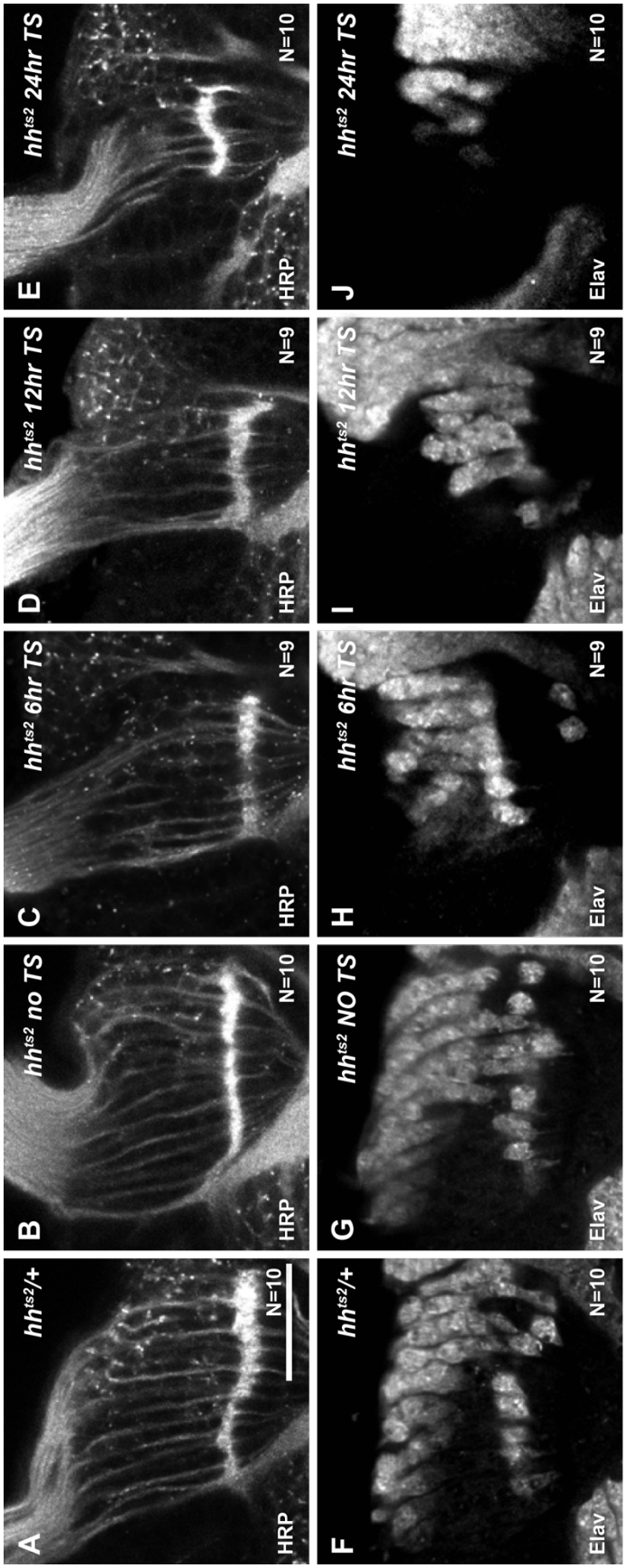
A
hh^ts2/+
HRP
N=10
B
hh^ts2 no TS
HRP
N=10
C
hh^ts2 6hr TS
HRP
N=9
D
hh^ts2 12hr TS
HRP
N=9
E
hh^ts2 24hr TS
HRP
N=10
F
hh^ts2/+
Elav
N=10
G
hh^ts2 NO TS
Elav
N=10
H
hh^ts2 6hr TS
Elav
N=9
I
hh^ts2 12hr TS
Elav
N=9
J
hh^ts2 24hr TS
Elav
N=10

Fig. S3: Fewer photoreceptors and lamina neurons develop when functional Hh availability is titrated. (A-E) Photoreceptor axons in the lamina were labelled with HRP in the following genotypes and conditions: **(A)** hh^{ts2}/+ shifted from the permissive temperature (18ºC) to the restrictive temperature (29ºC) for 24 hours, **(B)** hh^{ts2} raised at the permissive temperature, **(C-E)** hh^{ts2} shifted from the permissive temperature to the restrictive temperature for **(C)** 6 hours, **(D)** 12 hours, **(E)** 24 hours. **(F-J)**. All neurons were labelled with Elav for the same genotypes as (A-E). The pattern of neuronal differentiation worsened progressively with longer temperature shifts, with fewer neurons differentiating overall. Scale bar = 20µm.